PNAS RESEARCH ARTICLE | CELL BIOLOGY

Chlamydomonas FBB18 is a ubiquitin-like protein essential for the cytoplasmic preassembly of various ciliary dyneins

Ryosuke Yamamoto[a,1], Yui Sahashi[a,1,2], Rieko Shimo-Kon[a,1], Miho Sakato-Antoku[b,1], Miyuka Suzuki[a,3], Leo Luo[c,d], Hideaki Tanaka[e,4], Takashi Ishikawa[c,d], Toshiki Yagi[f], Stephen M. King[b], Genji Kurisu[a,e], and Takahide Kon[a,5]

Affiliations are included on p. 9.

Edited by Yale Goldman, University of California Davis, Davis, CA; received November 21, 2024; accepted February 14, 2025

Motile cilia are organelles found on many eukaryotic cells that play critical roles in development and fertility. Human CFAP298 has been implicated in the transport/assembly of ciliary dyneins, and defects in this protein cause primary ciliary dyskinesia. However, neither the exact function nor the structure of CFAP298 have been elucidated. Here, we took advantage of *Chlamydomonas*, a ciliated alga, to study the structure and function of FBB18, an ortholog of CFAP298. Multiple ciliary dyneins were greatly reduced in cilia of *Chlamydomonas fbb18* mutants. In addition, we found that both the stability of ciliary dynein heavy chains (HCs) and the association between HCs and intermediate/light chains (IC/LCs) are greatly reduced in *fbb18* cytoplasm, strongly suggesting that FBB18 functions in the cytoplasmic assembly (the so-called "preassembly") of dynein complexes from HC/IC/LCs. Furthermore, X-ray crystallography revealed that FBB18 forms a bilobed structure with globular domains at both ends of the molecule, connected by an α-helical bundle. Unexpectedly, one globular domain shows high similarity to ubiquitin, a small protein critical for the modification of a variety of protein complexes, and this ubiquitin-like domain is indispensable for the molecular function of FBB18. Our results demonstrate that FBB18, a specialized member of the ubiquitin-like protein family, plays a critical role in dynein preassembly, most likely by mediating diverse interactions between dynein HCs, molecular chaperone(s), and other preassembly factor(s) using the ubiquitin-like domain as well as other regions, and by facilitating the proper folding of dynein HCs.

cilia | dynein | ubiquitin | FBB18 (DAB2) | CFAP298 (DNAAF16/C21ORF59)

Significance

Dyneins are macromolecular machines composed of numerous subunits. Dynein species driving ciliary motility assemble in a complex cytoplasmic pathway mediated by various preassembly factors. Defects in this process lead to primary ciliary dyskinesia (PCD) in humans which involves infertility, bronchial problems, *situs inversus,* and other symptoms. Here, we use X-ray crystallography to show that FBB18, the *Chlamydomonas* ortholog of the PCD protein CFAP298, is a unique Type-II ubiquitin-like protein (UBL) specialized for dynein preassembly. This UBL is essential for the progression of the cytoplasmic assembly pathway of these motor–protein complexes. Our findings enhance the understanding of the complex molecular mechanisms underlying dynein holoenzyme formation in the cytoplasm as well as the detailed pathology of human PCD linked to CFAP298 defects.

Motile cilia are complex organelles consisting of more than ~ 600 proteins, and their movement is critical for numerous aspects of eukaryotic biology including normal development, fertility, and infection prevention (1–6). Ciliary motility is driven by motor–protein complexes called "ciliary dyneins" (7–9), which are located on the doublet microtubules inside cilia. They are classified into two groups: the outer arm dynein (ODA) and the inner arm dynein (IDA), and defects in these dyneins in higher eukaryotes cause complex diseases collectively called primary ciliary dyskinesia (PCD) (10–12).

Ciliary dyneins are preassembled in the cytoplasm from their numerous subunits (heavy chains: HCs, intermediate chains: ICs, light chains: LCs) (13–15), and then loaded onto the intraflagellar transport (IFT) machinery and transported into cilia (16–18). Dynein preassembly is a sequential and complicated process (14, 15, 19), and many aspects of the precise molecular mechanisms of preassembly remain to be elucidated. Only recently, several proteins (dynein preassembly factors) have been identified and reported to play a role in this complicated sequential process (14, 20).

CFAP298 [also known as DNAAF16 or C21ORF59, for nomenclature see (21)] is a protein of unknown function/structure containing a DUF2870 domain (*SI Appendix*, Fig. S1), that was first identified in screens for PCD-causing mutations/variants/proteins in zebrafish and humans (22). Interestingly, ciliary ODAs were particularly deficient in the zebrafish knockdown strain of CFAP298, and CFAP298 was hypothesized to function as an adapter between ciliary dyneins and the IFT machinery. Also, CFAP298 has been linked to adolescent idiopathic scoliosis in zebrafish, possibly due to the impaired motility of the brain cilia (23). In addition, a recent study showed that CFAP298 is important for both ciliary motility and length regulation in the ciliate *Euplotes vannus* (24). However, the exact molecular function(s) of CFAP298 in ciliogenesis, as well as the structural basis of the cilia-related function(s) of this protein, remain to be elucidated.

In this study, to further analyze the molecular function of CFAP298, we performed mutational analysis of the *Chlamydomonas* ortholog of CFAP298, flagellar-basal body protein 18 [FBB18, also known as DAB2 (25); hereafter, we will primarily use FBB18 as

The authors declare no competing interest.

This article is a PNAS Direct Submission.

[1]R.Y., Y.S., R.S.-K. and M.S.-A. contributed equally to this work.

[2]Present address: No current academic affiliation.

[3]Present address: Department of Chemistry, Graduate School of Science, Osaka University, Osaka 567-0047, Japan.

[4]Present address: TechnoPro, Inc., TechnoPro R&D Company, Hyogo 650-0047, Japan.

[5]To whom correspondence may be addressed. Email: kon.takahide.sci@osaka-u.ac.jp.

This article contains supporting information online at https://www.pnas.org/lookup/suppl/doi:10.1073/pnas.2423948122/-/DCSupplemental.

Published March 19, 2025.

a designation] (*SI Appendix*, Fig. S1). We have found that an *fbb18* mutant (*fbb18-2*) exhibits reduced swimming due to ciliary defects in several ciliary dynein species. In addition, in *fbb18-2* cytoplasm, dynein HCs were unstable and ciliary dyneins could not form a complete complex, strongly suggesting that FBB18 functions in dynein preassembly, specifically in the proper folding of dynein HCs. Furthermore, we solved the crystal structure of FBB18 at 2.3 Å resolution, which revealed that FBB18 has a bilobed structure with globular domains at both ends of the molecule bridged by a central three-helix bundle. Surprisingly, one of the globular domains shows high similarity to ubiquitin, a protein critical for protein modification (26–31) and known for its role as a marker for the degradation of various protein complexes. We have also shown that this ubiquitin-like domain is functional in dynein preassembly.

These findings demonstrate that FBB18 is a unique ubiquitin-like protein (UBL) specialized for dynein preassembly and provide important insights into the function and structure of the human PCD protein CFAP298, the higher eukaryotic ortholog of FBB18.

Results and Discussion

***Chlamydomonas* FBB18, an Ortholog of CFAP298, Is Important for Proper Cell/Ciliary Motility.** CFAP298 is conserved from algae to humans (*SI Appendix*, Fig. S1), and in higher eukaryotes, defects in this protein cause PCD due to loss of ciliary dyneins, particularly ODAs (22). However, neither its detailed molecular function(s) nor its exact three-dimensional structure are known. Here, we first performed a mutational analysis of FBB18, the *Chlamydomonas* ortholog of CFAP298. FBB18 is a protein of 277 amino acids with a predicted MW of 30,884 (*SI Appendix*, Fig. S1), and we obtained and analyzed an uncharacterized allele of *fbb18* [*fbb18-2*, the original mutant strain (LMJ.RY0402.149043) was obtained from the CLiP library (https://www.chlamylibrary.org/) (32), see also *SI Appendix*, Table S1] (Fig. 1*A*). The *fbb18-2* mutant has the *aphviii* insertional marker in the last (8th) exon of the *FBB18* gene (32), but we did not observe a shorter fragment of the FBB18 protein in the whole-cell samples of *fbb18-2* by Western blots (Fig. 1*B*). The shorter fragment of FBB18 was not observed even in 4 × overloaded samples of *fbb18-2*, strongly suggesting that *fbb18-2* is a null mutant like the previously reported *fbb18-1* (33).

We found that the *fbb18-2* mutant cells grew cilia and were able to swim in early log phase cultures. However, they exhibited slower swimming velocity and lower ciliary beat frequency compared to WT (Table 1), suggesting that ciliary dyneins in *fbb18-2* generate less propulsive force (34, 35). We also noticed that *fbb18-2* cells eventually became unciliated and could barely swim in old cultures. The Fbb18-motility phenotype cosegregated with the *aphviii* insertional marker in the 22/22 meiotic progeny from crosses between *fbb18-2* and WT, and all *fbb18-2* mutant progeny showed a similar motility phenotype. Ectopic expression of the WT FBB18 protein with a 3HA tag partially rescued the motility phenotype of *fbb18-2* (Fig. 1*A* and Table 1) in the rescued strain (*fbb18; FBB18:3HA:PSADPRO-TG*). The expression of the epitope-tagged FBB18 (FBB18:3HA-TG) in the rescued strain was lower than that of the endogenous FBB18 protein in WT (Fig. 1 *A* and *B*), which may be one reason why the motility of the rescued strain was only partially restored (Table 1). The reason for the low expression of the FBB18:3HA-TG protein is unclear, but the addition of the 3HA tag at the C-terminus may affect the stability of the FBB18 protein in cells. Taken together, these results strongly suggest that the motility phenotype of *fbb18-2* is caused by the insertional mutation in the *FBB18* gene.

FBB18 Is Essential for Ciliary Assembly of Several Dynein Species. The observed slow-swimming phenotype of *fbb18-2* strongly suggested that some ciliary dyneins were missing or reduced in this mutant, and electron microscopic observation of cilia from the original *fbb18-2* mutant indeed revealed altered forms of ODAs and reduced IDAs (Fig. 1*C*). Spectral-counting mass spectrometry revealed that among ciliary dynein species (8, 38, 39), ODAα and a minor dynein (DHC3) were particularly reduced in *fbb18-2* cilia (Fig. 1*D*). IDAs b, c and e and three other minor dyneins (DHC4, DHC11, and DHC12) also showed a modest reduction (Fig. 1*D*). However, in contrast to multicellular eukaryotic mutants of CFAP298 (22, 40), the β and γ HCs of ODA (ODAβ and ODAγ) were apparently normal in *Chlamydomonas fbb18-2* cilia (Fig. 1*D*); metazoans lack an ODAα ortholog. The dynein defects observed in *fbb18-2* are similar to those observed in *fbb18-1* (33). However, *fbb18-1* has been described as immotile/palmelloids (33), whereas *fbb18-2* is able to swim in early log phase cultures. The reason(s) for this phenotypic discrepancy is unclear, but differences in experimental conditions such as cell culture methods, time of observation, and/or an additional mutation affecting ciliogenesis could underlie this discrepancy.

We also noticed that the cilia ratio in *fbb18-2* (~ 76%) was slightly lower than that of WT (~ 91%) (Table 1), and the ciliary length in *fbb18-2* was slightly shorter than that of WT [7.8 ± 1.3 μm (*fbb18-2*) vs 9.9 ± 1.5 μm (WT), n (cilium) = 80]. Since combined defects in ODAs and IDAs are often associated with both shorter ciliary length and a lower cilia ratio (41–44), the observed ciliary phenotypes of *fbb18-2* (short cilia/low cilia ratio)

Table 1. Motility/ciliary phenotypes of WT and the *fbb18-2*-related mutants

Strain Name /Nomenclature	Swimming Velocity (μm/s) [n (cell) = 80]	Beat Frequency (Hz)* [n (measurement) = 3]	Moving Distance /Beat Cycle†	Cilia Ratio (%)‡ [n (cell) = 200]
WT	140.7 ± 24.8	56.7 ± 2.1	2.48	90.8 (363 cilia)
fbb18-2 (A1)	61.8 ± 14.1	46.3 ± 3.5	1.33	75.5 (302 cilia)
fbb18; FBB18:3HA:PSADPRO-TG (B3S)	95.8 ± 18.9	55.3 ± 3.5	1.73	85.5 (342 cilia)
fbb18; FBB18$^{K184R/G212A}$:3HA:PSADPRO-TG (B3)	54.2 ± 13.7	50.0 ± 4.4	1.08	67.3 (269 cilia)
fbb18; FBB18$^{K201A/T202A/K203A}$:3HA:PSADPRO-TG (H3)	56.6 ± 12.2	50.0 ± 2.6	1.13	76.8 (307 cilia)

*Ciliary beat frequency was measured by analyzing the fluctuation of a large population of cells using the Fast Fourier Transform analyzer (36).
†Calculated by dividing the "average swimming velocity" by the "average beat frequency." This is a parameter of the ciliary waveform/bend angle (37).
‡Calculated by visually counting the number of cilia on 200 cells for each strain [if cells are fully and ideally ciliated, the number of cilia should be 400 (100%)].

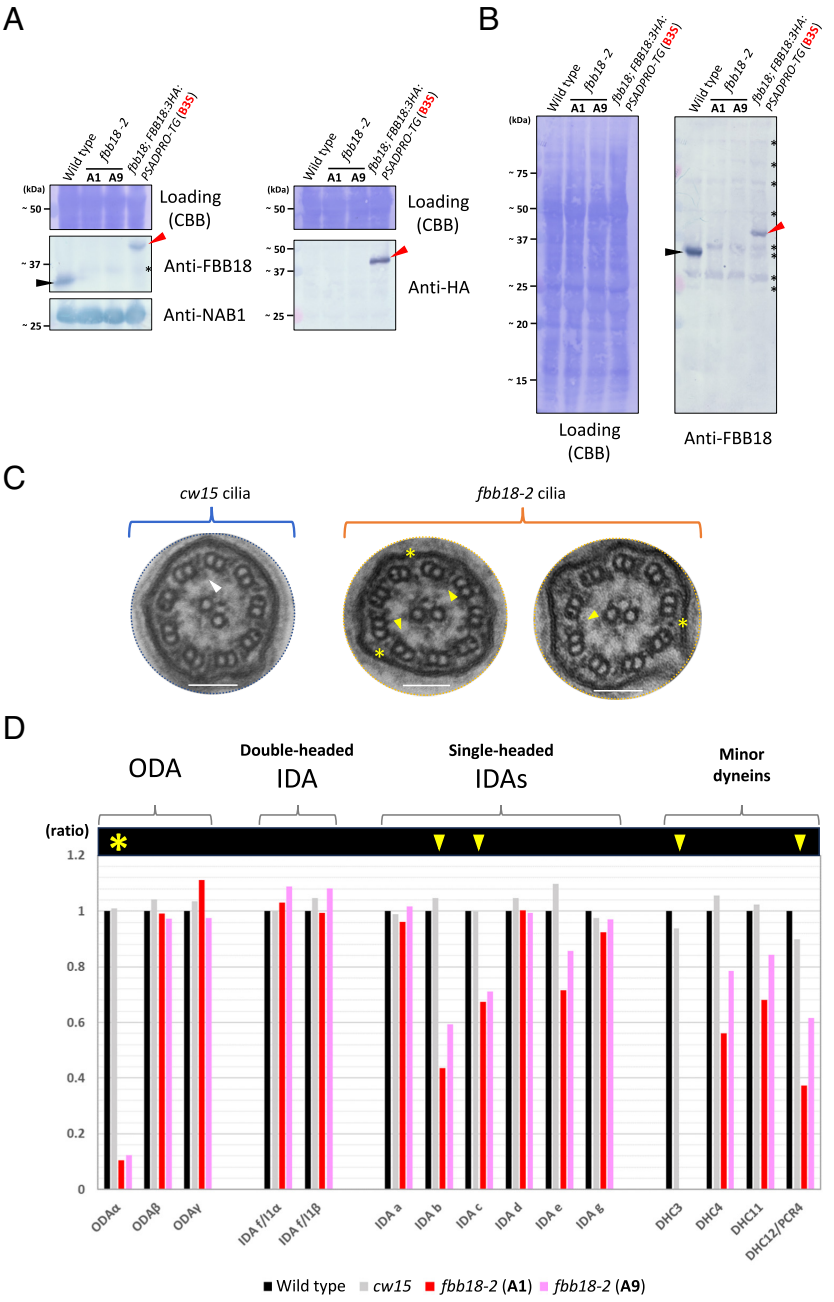

Fig. 1. Characterization of the *Chlamydomonas fbb18-2* mutant (*A*) Western blots of whole-cell samples from wild type (WT), *fbb18-2* (A1 and A9), and the rescued strain (B3S). A black arrowhead indicates the FBB18 protein in WT and red arrowheads indicate the epitope-tagged FBB18 protein (FBB18:3HA-TG) in the rescued strain (B3S) (black asterisk: unidentified nonspecific band: This band is covered by the strong WT FBB18 signal, but we have confirmed the presence of this band in some overloaded WT blots. Also, this band is sometimes absent in *fbb18-2* samples and may represent a ~ 35-kDa protein with variable expression levels depending on sample preparation). (*B*) Western blot of whole-cell samples from WT, *fbb18-2* (A1 and A9), and the rescued strain (B3S) on a hard (12%) gel. A black arrowhead indicates the FBB18 protein in WT and a red arrowhead indicates the epitope-tagged FBB18 protein (FBB18:3HA-TG) in the rescued strain (B3S). Short FBB18 fragments cannot be observed in the *fbb18-2* samples, suggesting that *fbb18-2* is a null mutant (black asterisks: nonspecific bands). (*C*) Transmission electron microscopic images of the *cw15* and *fbb18-2* (CLiP; LMJ.RY0402.149043) cilia. In *fbb18-2*, densities of IDAs appear to be reduced/altered on some doublet microtubules (yellow arrowheads) compared to *cw15* (white arrowhead), which is regarded as WT for ciliary composition. Also, we sometimes observed ODAs in altered forms (yellow asterisks) in *fbb18-2*. (Scale bars, ~ 100 nm.) (*D*) Summary of the spectral counting analyses of ciliary axonemal dyneins from WT, *cw15,* and two *fbb18-2* mutants (A1 and A9). Yellow asterisk/arrowheads indicate dynein species for which spectral counts were reduced by more than 25% in the both *fbb18-2* mutants compared to WT.

could be attributed to a combined defect in ODAα, IDAs b, c and e, and minor dyneins in *fbb18-2* cilia (Fig. 1*D*). The ciliary phenotypes of *fbb18-2* are milder than those of mutants that completely lack both ODA and some IDA species, most likely because *fbb18-2* does not completely lack the affected dynein species in cilia, but at least retains some amounts of them.

FBB18 Is Primarily Localized to the Cell Body and Is Important for the Stability of Ciliary Dynein HCs in the Cytoplasm. In the previous report, FBB18, as well as its higher eukaryotic ortholog CFAP298 (*SI Appendix*, Fig. S1), was hypothesized to function as an IFT adapter between ciliary dyneins and the IFT machinery in cilia (22). Loss of one IFT protein is known to often cause instability

of other IFT component(s) (45–47), but we found that two IFT-related mutations (*ift46* and *ift74*) did not significantly affect the stability of FBB18 (Fig. 2*A*), casting doubt on the hypothesized IFT-related role of FBB18 in cilia. Therefore, we next sought to determine in which cellular fraction FBB18 is primarily localized in WT *Chlamydomonas*. Interestingly, we found that most of the FBB18 protein is located in the cell body (containing the cytoplasm) and only trace amounts of FBB18, if any, are present in cilia (Fig. 2*B*). This FBB18 localization is consistent with previous reports of CFAP298 localization, all of which reported CFAP298 localization in the cytoplasm but not in cilia (40, 48, 49), and also with the previous study of FBB18 (33), but is inconsistent with a potential function of FBB18 as an IFT adaptor.

Based on the cytoplasmic localization of FBB18, we hypothesized that FBB18 has a specific cytoplasmic role related to ciliogenesis, and explored its association with ciliary dynein complexes in the cytoplasm. To our surprise, the amount of ciliary dynein HCs in *fbb18-2* cytoplasm was greatly reduced compared to WT (Fig. 2*C* and *SI Appendix*, Table S2), strongly suggesting that the stability of dynein HCs is reduced in *fbb18-2*. Such instability of dynein HCs has been observed in the cytoplasm of preassembly mutants, in which dynein HCs are unfolded/misfolded and most likely selectively degraded (52–54). In contrast to HCs, the amounts of most ciliary dynein IC/LCs in *fbb18-2* cytoplasm appeared relatively normal compared to WT (Fig. 2*C* and *SI Appendix*, Table S2), with only a few exceptions of reduced/accumulated IC/LCs [such reduction/accumulation of some kinds of dynein IC/LCs when HCs are unstable has also been previously observed in the cell body of dynein preassembly mutants, see (50–54)]. Given that different HCs of ciliary dyneins with discrete IC/LC composition are all affected in *fbb18-2* cytoplasm (Fig. 2*C* and *SI Appendix*, Table S2), our results strongly suggest that FBB18 functions in dynein preassembly, specifically in the folding of dynein HCs, and that unfolded/misfolded HCs are selectively degraded in *fbb18-2* cytoplasm, ultimately leading to the reduction of dynein amounts in *fbb18-2* cilia. Consistent with the idea that FBB18 functions in dynein preassembly, the observed motility and ciliary phenotypes, as well as the sequential changes in motility, of *fbb18-2* were strongly reminiscent of some previously reported preassembly mutants (50, 51, 53–55). Expression of the epitope-tagged FBB18 protein (FBB18:3HA-TG) was able to cause a clear partial rescue of these Fbb18-motility/ciliary phenotypes (Figs. 1 *A*, 2 *D* and Table 1).

Loss of FBB18 Strongly Attenuates the Efficiency of Dynein Preassembly. To directly test the hypothesis that FBB18 functions in dynein preassembly, we evaluated the efficiency of preassembly in *fbb18-2* cytoplasm using a gel filtration column chromatography. The elution peak containing the preassembled–dynein complexes was much lower in *fbb18-2* than in WT, indicating that the efficiency of dynein preassembly is indeed much lower in *fbb18-2* (Fig. 3 *A* and *B*). To investigate the preassembly state of ciliary dynein complexes in *fbb18-2* cytoplasm, we then selected the ODA complex as a representative of ciliary dynein complexes, and the amounts of ODA subunits (ODAα/ODAβ/ODAγ HCs, IC2, LC1, and LC3) in the elution fractions were evaluated by Western blots. We found that the quantitative ratio of preassembled (early fractions) to free (late fractions) IC/LCs is low in *fbb18-2* (Fig. 3*B*) compared to WT (Fig. 3*A*), indicating both the low efficiency of dynein preassembly and the weak association between HCs and IC/LCs in *fbb18-2*. We also failed to detect ODAα in the *fbb18-2* elution fractions (Fig. 3*B*), consistent with the highly reduced and unstable nature of this HC in *fbb18-2* cytoplasm (Fig. 2*C* and *SI Appendix*, Table S2). On the other hand, in *fbb18-2*, although the amounts were lower (Fig. 2*C* and *SI Appendix*, Table S2), ODAβ and ODAγ could be detected in the elution blots (Fig. 3*B*), probably forming the unusual ODA complex without ODAα. The formation of the unusual ODA complexes is consistent with our observations of both altered ODA forms in *fbb18-2* cilia and greatly reduced levels of ODAα spectra in *fbb18-2* cilia (Fig. 1 *C* and *D*) [such an unusual ODA complex without ODAα is also formed in *oda11*, a mutant with a defect in the *DHC13* (ODAα) gene (56)]. Taken together, these results clearly demonstrate that loss of FBB18 severely reduces the efficiency of dynein-complex formation from each dynein subunit in the cytoplasm, ultimately causing both the ciliary dynein and motility defects observed in *fbb18-2* (Fig. 1 *C* and *D* and Table 1).

Unique Bilobed Structure of FBB18 Revealed by X-ray Crystallography. To investigate the structural basis of the molecular function of FBB18 in dynein preassembly, we attempted to solve the crystal structure of the FBB18 molecule. To this end, we overexpressed the full-length 6His:FBB18 protein as well as several deletion mutants in *Escherichia coli* and purified them by nickel-affinity and gel filtration column chromatography (*SI Appendix*, Fig. S2 *A–D*). All of the proteins obtained were about 70 ~ 90% pure judging from the SDS-PAGE analysis and were concentrated to 20 ~ 45 mg/mL without showing any sign of precipitation. However, only one mutant (6His:FBB18del4, hereafter called "FBB18del4"; *SI Appendix*, Fig. S2 *A* and *B*) readily crystallized and was thus chosen for further structural analysis (see also *SI Appendix*, *Supplemental Materials and Methods*). The FBB18del4 mutant lacks the last 59 amino-acid residues at the C-terminus and was successfully crystallized, presumably due to the loss of the flexible/intrinsically disordered region. Then, using the BL44XU beamline at SPring-8, we obtained X-ray diffraction data both for native (*SI Appendix*, Fig. S2 *A* and *B*) and selenomethionine-derivative (*SI Appendix*, Fig. S2 *C* and *D*) crystals of FBB18del4 at 2.3 Å and 2.6 Å resolution, respectively. The diffraction data were first processed using XDS (58, 59), and the initial phase of the selenomethionine derivative (*SI Appendix*, Fig. S2 *C* and *D*) was determined by single-wavelength anomalous dispersion using AutoSol in the PHENIX software (60, 61). Next, a structural model was constructed for one of the four FBB18del4 molecules present in the crystallographic asymmetric unit. The constructed model was used as a search model, and by applying the molecular replacement method against the diffraction data of the native crystal, we gained a high-quality electron density map. After iterative model building and refinement, the crystal structure of FBB18del4 was determined at 2.3 Å resolution. Each one of the four FBB18del4 molecules in the crystallographic asymmetric unit has a very similar structure (RMSD = ~ 0.2 to 0.5 Å). In this report, we focus primarily on molecule A, for which we were able to perform the best model building, and in which 215 of the 218 FBB18 amino acid residues in FBB18del4 were traced.

The FBB18 molecule is mainly composed of nine α-helices (α1 ~ α9) and five β-strands (β1 ~ β5) and shows a bilobed structure, in which a three-helix bundle (α1, α4, and α6) forms a shaft of the protein with two globular domains placed at each end of the shaft (Fig. 4*A*). One of the two globular domains consists mainly of long loop structures present between α1 and α4 as well as α6 and α7, while the other globular domain is composed mainly of a mixed five-stranded β-sheet (β1 ~ β5), two short α-helices (α8 and α9), and a portion of the α1 helix elongating from the central three-helix bundle.

The solved FBB18 structure has a characteristic surface charge distribution. Half of the FBB18 molecule containing the loop-rich globular domain is generally negatively charged, while the other half of the molecule is predominantly positively charged, making the overall charge distribution of the FBB18 molecule highly asymmetric (Fig. 4*B*). In addition, a belt-like extended hydrophobic

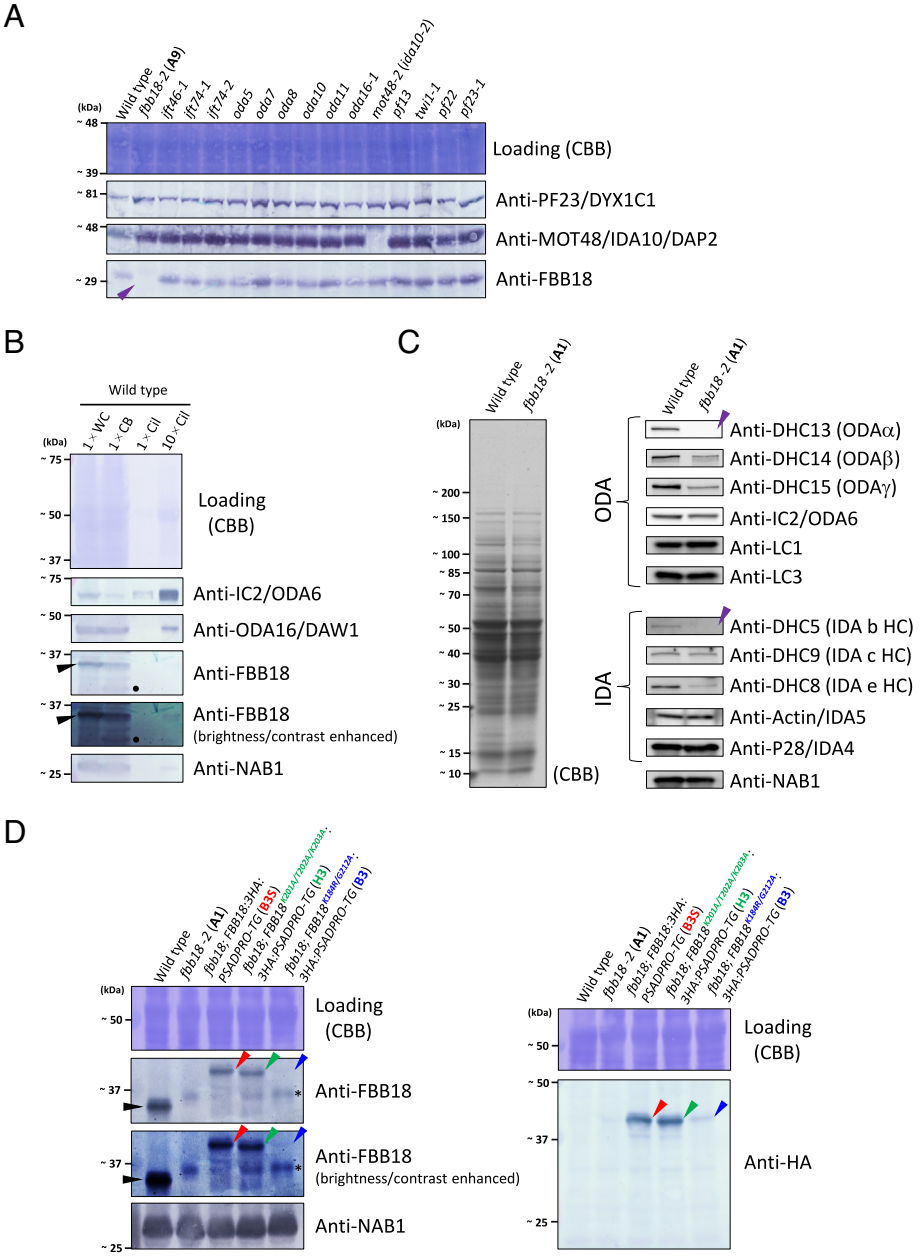

Fig. 2. FBB18 is localized to the cell body and loss of FBB18 causes instability of dynein HCs in the cytoplasm (*A*) Western blots of whole-cell samples from various preassembly and IFT-related mutants. The *fbb18-2* (A9) mutant lacks the FBB18 band (purple arrowhead), while having apparently normal levels of PF23 and MOT48, other known preassembly factors (50, 51). All mutants except for *fbb18-2* had FBB18, although the amounts varied slightly from strain to strain, and two IFT-related mutations (*ift46* and *ift74*) do not appear to affect the stability of the FBB18 protein. (*B*) Western blots of whole-cell (1 × WC), cell-body (1 × CB), cilia (1 × Cil), and 10-fold concentrated cilia (10 × Cil) samples from WT. The stoichiometry of whole cell, cell body, and cilia is approximately the same as in the 1 × samples. The FBB18 proteins are mainly localized to the cell body (containing the cytoplasm) in *Chlamydomonas*, and only very small amounts of FBB18 are found in cilia. This localization of FBB18 is in contrast to that of IC2, a subunit of ODA. During sample preparation, FBB18 is easily degraded in the cell body deciliated by dibucaine, and both intact FBB18 (black arrowheads) and partially degraded FBB18 (black circles) are observed in the blot. (*C*) CBB-stained gel (*Left*) and Western blots (*Right*) of the cytoplasmic extracts from WT and *fbb18-2* (A1) using various dynein-subunit antibodies. While the amounts of ciliary dynein IC/LCs in the cytoplasmic extract appear normal to only slightly reduced in *fbb18-2* compared to WT, the amounts of dynein HCs with different IC/LC compositions are all reduced in *fbb18-2* compared to WT, although the degree of reduction (slight/moderate/severe) varies depending on the HC species. In particular, ODAα (DHC13) and IDA b HC (DHC5) are almost undetectable in these Western blots (purple arrowheads). These results strongly suggest that FBB18 is important for the stability of dynein HCs in the cytoplasm. (*D*) Western blots of whole-cell samples from WT, *fbb18-2* (A1), the rescued strain (B3S), transformed *fbb18-2* strain (H3) expressing the epitope-tagged mutant FBB18 protein (FBB18$^{K201A/T202A/K203A}$:3HA-TG), and transformed *fbb18-2* strain (B3) expressing the other epitope-tagged mutant FBB18 protein (FBB18$^{K184R/G212A}$:3HA-TG). Black arrowheads indicate the WT FBB18 protein and red arrowheads indicate the FBB18:3HA-TG protein in the rescued strain (B3S). The green arrowheads indicate the FBB18$^{K201A/T202A/K203A}$:3HA-TG protein, which is expressed in the H3 strain at almost the same level as the FBB18:3HA-TG protein (red arrowheads) in the rescued strain (B3S). On the other hand, the FBB18$^{K184R/G212A}$:3HA-TG protein is very weakly expressed in the B3 strain at levels close to the detection limits in the blots (blue arrowheads) (black asterisks: nonspecific bands).

surface was found along the long axis of the FBB18 molecule, parallel to the shaft-forming three-helix bundle (Fig. 4*C*). The characteristic feature of the FBB18 molecule may contribute to the interaction between FBB18 and its interacting partner(s), as mentioned later in this report.

FBB18 Is a Unique Member of the Type-II UBLs. Using the solved structure of FBB18del4 as a query, we performed a structural similarity search on the DALI server (http://ekhidna2.biocenter.helsinki.fi/dali/). Surprisingly, we found that one globular domain with the mixed five-stranded β-sheet has a β-grasp fold and shows high similarity

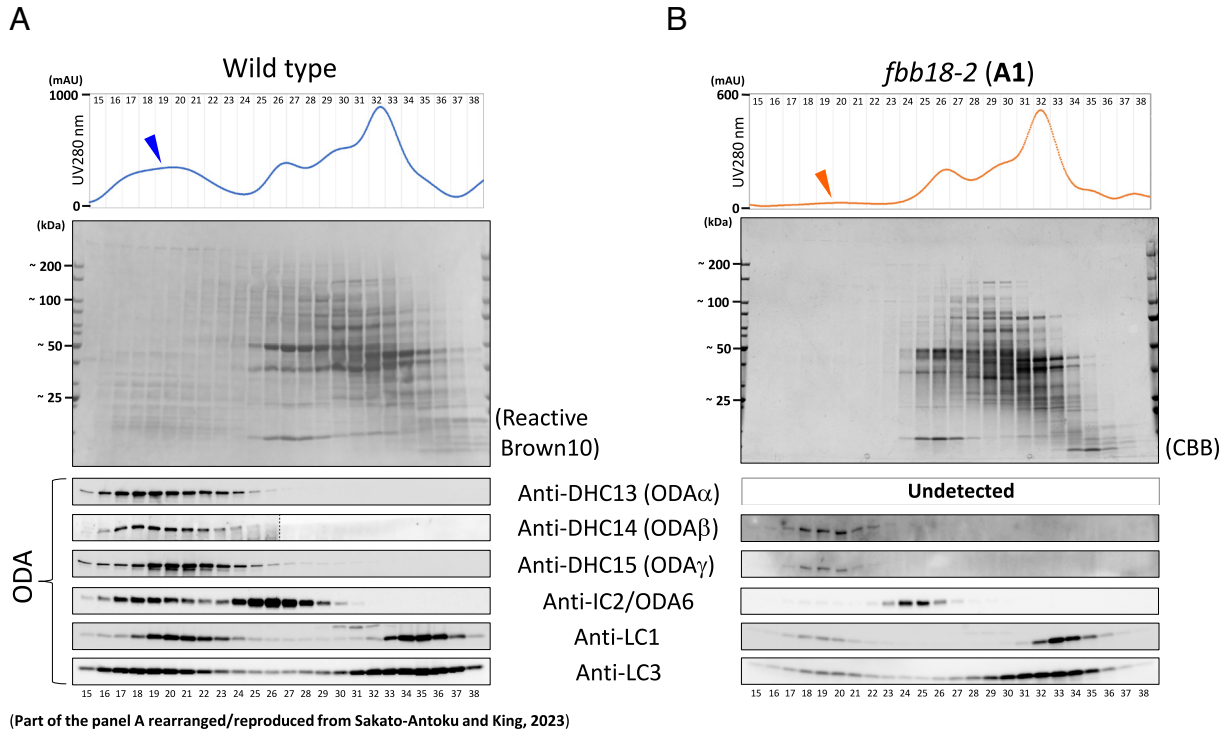

Fig. 3. In *fbb18-2*, the cytoplasmic preassembly of ciliary dyneins is strongly attenuated (*A* and *B*) Gel filtration (Superose 6 HR 10/30) elution profiles (*Top*), stained membrane/gel (*Middle*), and Western blots of elution fractions using different ODA-subunit antibodies (*Bottom*) of cytoplasmic extracts [WT and *fbb18-2* (A1) are (*A*) and (*B*), respectively, in this figure]. A peak containing the preassembled-dynein complexes is present in the early fractions of WT (blue arrowhead), whereas the peak becomes very low in *fbb18-2* (orange arrowhead), indicating that the amount of preassembled-dynein complexes in *fbb18-2* cytoplasm is low. In addition, the quantitative ratio of preassembled (early fractions) to free (late fractions) ODA IC/LCs is low in the *fbb18-2* extract compared to WT, strongly suggesting that the efficiency of dynein preassembly in the cytoplasm is also low in *fbb18-2*. In the cytoplasm of *fbb18-2*, the ODA complex without ODAα can be assembled, and this result is consistent with the results for ciliary axonemal dyneins shown in Fig. 1*D*. The dotted line on the WT ODAβ/DHC14 sample indicates the combining of two different blots, and the WT data in (*A*) in this figure [a Reactive Brown 10-stained nitrocellulose membrane and all blots (ODAα/DHC13, ODAβ/DHC14, ODAγ/DHC15, IC2, LC1, and LC3)] were published previously (57) and are rearranged and reproduced here under a CC BY-NC 4.0 license (author reuse) and with permission of the publisher (ASCB).

to ubiquitin, a small protein critical for modification/degradation/targeting of various protein complexes (26–31) (Figs. 4 *A* and 5 *A*). On the other hand, the opposite globular domain with long loops (Fig. 4*A*) did not show any substantial structural similarity to known proteins. The similarity between ubiquitin and human CFAP298 has been only recently predicted using a homology-detection algorithm (65), and we definitively and experimentally show that *Chlamydomonas* FBB18 is a specialized member of the UBL family. Hereafter, we call the globular domain with ubiquitin similarity as the "ubiquitin-like domain," and the opposite globular domain with the loop-rich structure as the "loop domain." The bilobed structure of the FBB18 molecule (Fig. 4*A*) can be interpreted as an evolutionarily modified version of the ubiquitin fold, with a large structural unit consisting of the central shaft-forming three-helix bundle and the loop domain inserted into the β-grasp fold of the ubiquitin-like domain.

Many UBL-family proteins (Type-I UBLs), like conventional ubiquitin, covalently bind to lysine residues in target proteins to regulate their activity, stability, and subcellular localization (67). In addition, some UBLs, such as small ubiquitin-like modifier, form covalently linked polymers like ubiquitin to achieve more diverse regulation of target proteins (67, 68). In the ubiquitin-like domain of FBB18, residues involved in the above-mentioned covalent binding/linking appear to be superficially conserved [such as M1, K184, K201, and G212; hypothesized from the multiple sequence alignment (69) and the solved FBB18 structure, Fig. 5*A*]. However, structural and biochemical features of the FBB18 molecule suggest that FBB18 does not undergo such covalent protein modifications: In the FBB18 molecule, the glycine residue (G212; corresponding to G76 of human ubiquitin), a possible donor for covalent binding, is not located at the C-terminus of the protein but in the middle of the polypeptide chain and therefore cannot contribute to covalent bond formation (Fig. 5*A* and *SI Appendix*, Fig. S1). Also, in Western blots of *Chlamydomonas* cytoplasmic extract or whole-cell samples, only signals corresponding to monomeric FBB18 were detected by the FBB18 antibody, and we did not observe signals corresponding to high-molecular-weight FBB18 complexes formed by covalent polymerization or covalent binding to other proteins. In addition, mutations/variants of FBB18/CFAP298 beyond G212 in the C-terminal regions of these proteins (*SI Appendix*, Fig. S1) have been shown to affect the molecular function of FBB18 (33) or cause PCD in humans (22), suggesting that the C-terminal regions are important for the molecular functions of FBB18 as well as CFAP298. Therefore, FBB18 most likely belongs to the Type-II UBL family, i.e., UBLs that bind and regulate their target proteins through noncovalent interactions (67, 70).

Both the Ubiquitin-Like and Loop Domains Are Critical for the FBB18 Functions. Next, we performed structure-based mutational analysis to investigate the functional significance of the ubiquitin-like domain in the FBB18 molecule. Here, we focused on the outermost loop region (K201–K203; *SI Appendix*, Fig. S3*A*) of the ubiquitin-like domain. This loop is the most structurally polymorphic region among the four FBB18 molecules in the crystallographic asymmetric unit (Fig. 5*B*) and judging from the high B-factor (Fig. 5*C*), it is likely to be a highly mobile region, but also a highly evolutionarily conserved region among the FBB18 orthologs (*SI Appendix*, Figs. S1 and S3*A*). When the mutant FBB18:3HA-TG protein (FBB18$^{K201A/T202A/K203A}$:3HA-TG),

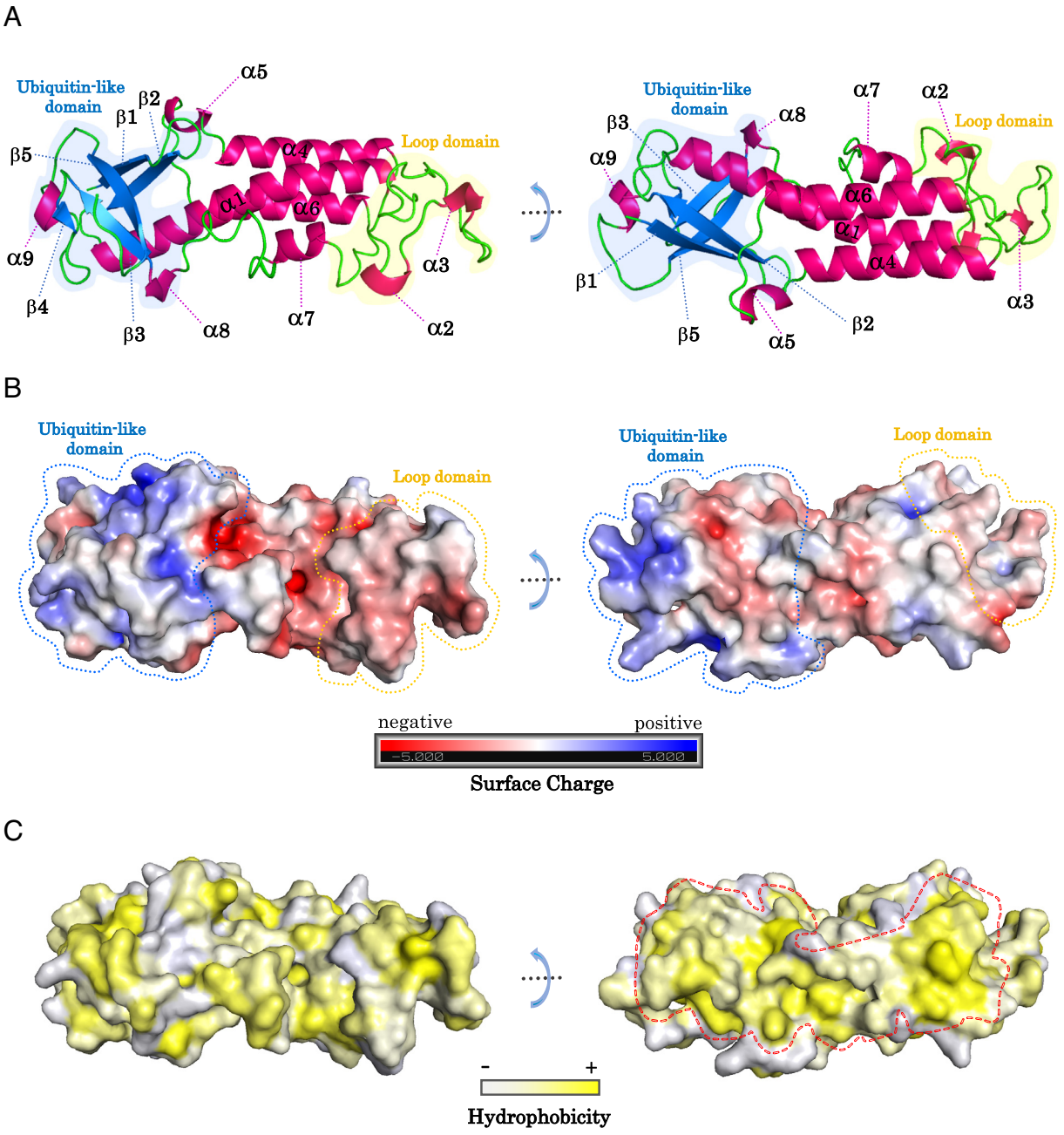

Fig. 4. *Chlamydomonas* FBB18 is a bilobed molecule (*A*) A ribbon diagram of the secondary structures of FBB18del4 determined by the DSSP plugin (62) in PyMOL. α-helices (α1 ~ α9) are shown in dark pink, and β-strands (β1 ~ β5) are shown in blue. The ubiquitin-like domain (*Left*, transparent blue) and the loop domain (*Right*, transparent yellow) are connected by a middle shaft composed of the three-helix bundle (α1, α4 and α6). (*B*) Display of surface charges of FBB18del4 predicted by the APBS plugin (63) in PyMOL. Strong positive charges (blue) are observable in the ubiquitin-like domain, while negative charges (red) are present around the loop domain, making the charge distribution of this protein highly asymmetric. (*C*) Display of hydrophobic surfaces of FBB18del4 predicted by the PyMOL script [Color_hy, a manually modified version of Color_h (64)]. The molecule has a belt-like extension of hydrophobicity (yellow) along its long axis (*Right*, circled in a red dotted line). The orientations of the FBB18del4 structures in (*B*) and (*C*) are the same as the orientations of the structures in (*A*) in this figure.

in which all these conserved residues (K201, T202, and K203) were replaced by alanine, was expressed in the *fbb18-2* mutant (*fbb18; FBB18*$^{K201A/T202A/K203A}$*:3HA:PSADPRO-TG*, Fig. 2*D* and *SI Appendix*, Table S1), its expression level was comparable to that of the WT FBB18:3HA-TG protein in the rescued strain (B3S) (Fig. 2*D*). However, expression of the mutant FBB18:3HA-TG protein in the *fbb18-2* mutant did not rescue the Fbb18-motility/ciliary phenotypes at all (Table 1). These results demonstrate the functional importance of this loop region in the ubiquitin-like domain and also clearly indicate that the ubiquitin-like domain of FBB18, a unique Type-II UBL protein, is functional in dynein preassembly and not just an evolutionary remnant.

In contrast to the ubiquitin-like domain, the loop domain located on the opposite side of the FBB18 molecule (Fig. 4*A*) is less evolutionarily conserved. However, it is also likely to play an important role in FBB18 function, i.e., preassembly of ciliary dynein complexes. This loop domain has a potentially mobile region with high B-factor/structural polymorphism (Fig. 5 *B* and *C*), as does the opposite ubiquitin-like domain. Strikingly, the corresponding residues of previously reported PCD/disease-related CFAP298 variants are mainly mapped to the loop domain of FBB18 (*SI Appendix*, Fig. S3*B*). Furthermore, our structural analysis using AlphaFold2 multimer (71) predicted that DHC5, HC of IDA b that is strongly reduced in both *fbb18-2* cilia and cytoplasm (Figs. 1 *D* and 2 *C* and

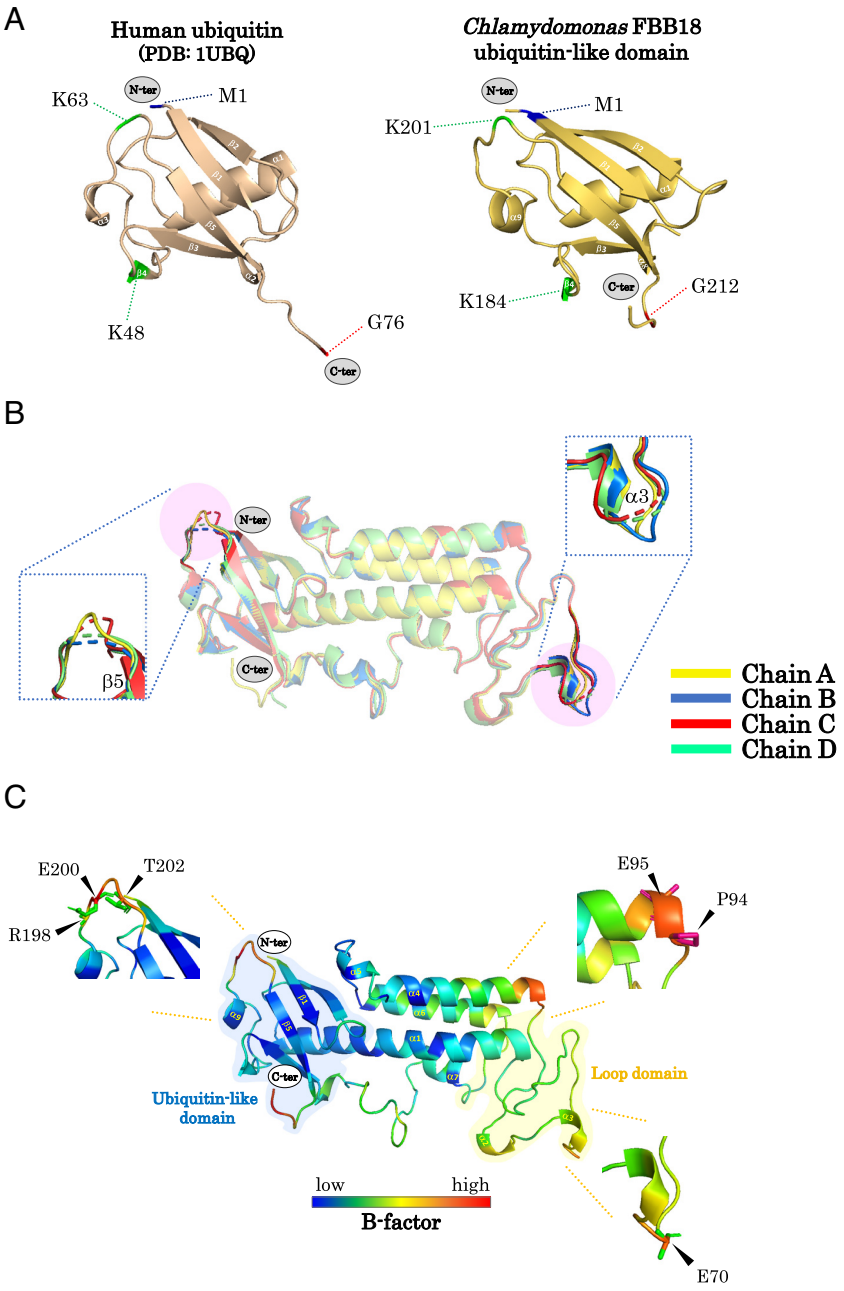

Fig. 5. FBB18 has a ubiquitin-like globular domain (*A*) Structural comparison between human ubiquitin [PDB: 1UBQ (66)] (*Left*) and the ubiquitin-like domain of FBB18del4 (*Right*). The ubiquitin-like domain of FBB18del4 has the mixed five-stranded β-sheet (β1 ~ β5) and three α-helices (α1, α8 and α9), which form a fold similar to the β-grasp fold of human ubiquitin. Residues important for polymerization in human ubiquitin and the hypothesized corresponding residues in *Chlamydomonas* FBB18del4 are also shown. For the functionality of this ubiquitin-like domain, see Fig. 2*D* and Table 1. (*B*) Alignment of the four FBB18del4 molecules (A ~ D) present in one crystallographic asymmetric unit. Regions with high variance were found both in the ubiquitin-like and loop domains [also shown in (*C*) in this figure], further indicating that these regions are intrinsically flexible. (*C*) Analyses of the B-factor in FBB18del4. Both the ubiquitin-like and loop domains have regions with high B-factor. These regions are presumed to represent flexible structures in the protein and are likely to act as binding interfaces between FBB18 and other protein(s) [ciliary dynein HCs, molecular chaperone(s), and other preassembly factor(s)].

SI Appendix, Table S2), binds to the vicinity of the loop domain of FBB18 (*SI Appendix*, Fig. S4 *A–D*). The interaction site was located at the end of the α6 helix near the loop domain of FBB18, which is also located in the belt-like extended hydrophobic surface of the FBB18 molecule found in this study (Fig. 4*C*). In addition, AlphaFold3 predictions showed higher confidence scores for certain parts/fragments of DHC5 than for the full-length DHC5 protein as potential interacting partners of FBB18 (*SI Appendix*, Table S3). There are several possibilities for the reason(s) for this observation, but it may indicate that additional regions of HC in the full-length DHC5 protein interfere with or weaken the interaction between DHC5 and FBB18, or that the full-length DHC5 protein adopts a different conformation from the parts/fragments of DHC5 that is less compatible with the small protein(s) like FBB18. Our observation also suggests that FBB18 is likely to bind to a partially folded form of DHC5, possibly during its preassembly. In particular, fragments containing the AAA2 module (part of the motor domain) of various ciliary dynein HCs, including DHC5 (*SI Appendix*, Fig. S4 *A–D*), had higher confidence scores as potential interaction partners for FBB18 than other regions of dynein HCs or associated IC/LCs (*SI Appendix*, Table S3). These results suggest that FBB18 primarily interacts with partially folded dynein HCs in vivo (for additional

predicted results from AlphaFold2/3 multimer, see *SI Appendix*, Fig. S5 *A–C* and Table S3).

Based on our biochemical, genetic, and structural analyses of FBB18 described above, and in light of the results of previous studies reporting many preassembly-related proteins as potential binding partners of FBB18 (as summarized in *SI Appendix*, Table S4), we propose that FBB18 facilitates the preassembly of ciliary dynein complexes by linking dynein HCs to molecular chaperone(s) and other preassembly factor(s) and helping these HCs to fold properly. This hypothesized role of FBB18 is consistent with the observed instability of HCs of various ciliary dynein species, with different IC/LC compositions, in *fbb18-2* cytoplasm (Fig. 2*C* and *SI Appendix*, Table S2), and also with the predictions of AlphaFold2/3 multimer (*SI Appendix*, Fig. S4 *A–D* and Table S3). Previous studies have suggested that in addition to dynein HCs, various preassembly factors, including MOT47, PF22, PF23, and ZMYND10, serve as interacting partners of FBB18 (or its orthologs) (*SI Appendix*, Table S4) and function in concert with FBB18. The two globular domains of FBB18 identified in this study, i.e., the ubiquitin-like domain and the loop domain (Figs. 4 *A* and 5 *A*), and their surrounding regions are strong candidates to act as an interaction interface and mediate the diverse interactions between FBB18, dynein HCs, and molecular chaperone(s)/preassembly factor(s). Determining the detailed interactome of FBB18, the specificity of FBB18 for interaction with various ciliary dynein subunits, and the precise molecular mechanism(s) of dynein preassembly performed by FBB18 and many other preassembly factors are important future projects for FBB18 research.

In conclusion, we have shown in this report that FBB18, a specialized Type-II UBL with a functional ubiquitin-like domain, plays a critical role in dynein preassembly. The unexpected finding of the dynein preassembly role of this unique Type-II UBL will facilitate our understanding of PCD associated with variants in CFAP298, the human ortholog of FBB18. Our results also shed valuable light on the molecular functions of UBL-family proteins, as well as on the origin and molecular evolution of the dynein preassembly pathway in eukaryotes.

Materials and Methods

***Chlamydomonas* Strains and Cultures.** *Chlamydomonas* mutant strains used in this study are summarized in *SI Appendix*, Table S1. The original *fbb18-2* mutant (LMJ.RY0402.149043) was obtained from the CLiP library (https://www.chlamylibrary.org/) (32). Several 137c-derivative strains (e.g. CC-124 and CC-125) were used as WT strains in this study for biochemical analyses. Regardless of the differences between mating types (72) and recently revealed genetic variance [e.g. (73, 74)], they were considered as WT as long as they show WT motility/ciliary phenotypes. Cells were grown on solid or in liquid Tris-Acetate-Phosphate media (75) under constant light or under a light/dark cycle (12/12 or 16/8 h). Details of other materials and methods, including the crystallization condition of FBB18, are fully described in *SI Appendix, Supplemental Materials and Methods*.

Data, Materials, and Software Availability. All other data are included in the manuscript and/or *SI Appendix*. Previously published data were used for this work in Fig. 3*A* (author reuse) from (57). We have obtained permission from the publisher (ASCB) to reuse it.

ACKNOWLEDGMENTS. We thank Dr. Ritsu Kamiya (Chuo University), Ms. Yu-Hsuan Chen (National Tsing Hua University), and Mr. Masahito Nagao/Yuya Yamasaki/Haruto Ijiri/Yu Kitamura (Osaka University) for their experimental assistance on the phenotypic analyses/observation of the *fbb18-2* mutants. We thank Drs. Keisuke Sakurai, Eiki Yamashita, and Atsushi Nakagawa (Osaka University) for their arrangement, assistance, and technical advice on the data collection of the FBB18 crystals on SPring-8 BL44XU beamline. This study was partially funded by grants from Uehara Memorial Foundation, Chubei Itoh Foundation, Japan Society for the Promotion of Science (JSPS) Grant-in-Aid for Young Scientists (B) (JP17K15117) and for Scientific Research (C) (JP20K06622 and JP24K09454) (to R.Y.), Swiss NSF (IZLIZ3_200294) (to T.I.), JSPS Grant-in-Aid for Scientific Research (C) (JP23K05723), for Scientific Research (B) (JP23K23190) and for Fund for the Promotion of Joint International Research (JP21KK0125) (to T.Y.), JSPS Grant-in-Aid for Scientific Research (B) (JP18H02390) (to G.K.), and JSPS Grant-in-Aid for Scientific Research (B) (JP26291034 and JP17H03665) (to T.K.). M.S-A. and S.M.K. were supported by grant R35-GM140631 from the NIH (to S.M.K.). The funders had no role in study design, data collection and analysis, decision to publish, or preparation of the manuscript.

Author affiliations: [a]Department of Biological Sciences, Graduate School of Science, Osaka University, Osaka 560-0043, Japan; [b]Department of Molecular Biology and Biophysics, University of Connecticut Health Center, Farmington, CT 06030-3305; [c]Department of Biology and Chemistry, Paul Scherrer Institute, Villigen 5232, Switzerland; [d]Department of Biology, ETH Zurich, Zurich 8093, Switzerland; [e]Institute for Protein Research, Osaka University, Osaka 565-0871, Japan; and [f]Department of Life and Environmental Sciences, Faculty of Bioresource Sciences, Prefectural University of Hiroshima, Hiroshima 727-0023, Japan

Author contributions: R.Y., S.M.K., and T.K. designed research; R.Y., Y.S., R.S.-K., M.S.-A., M.S., L.L., H.T., T.Y., S.M.K., G.K., and T.K. performed research; T.I., S.M.K., G.K., and T.K. administrated/supervised the study; and R.Y., T.I., S.M.K., and T.K. wrote the paper.

1. P. Satir, Cilia: Before and after. *Cilia* **6**, 1 (2017).
2. T. Ishikawa, Axoneme structure from motile cilia. *Cold Spring Harb. Perspect. Biol.* **9**, a028076 (2017).
3. N. A. Petriman, E. Lorentzen, Structural insights into the architecture and assembly of eukaryotic flagella. *Microb. Cell* **7**, 289–299 (2020).
4. T. Walton *et al.*, Axonemal structures reveal mechanoregulatory and disease mechanisms. *Nature* **618**, 625–633 (2023).
5. Z. Ren, X. Mao, S. Wang, X. Wang, Cilia-related diseases. *J. Cell. Mol. Med.* **27**, 3974–3979 (2023).
6. G. J. Pazour, Cilia structure and function in human disease. *Curr. Opin. Endocr. Metab. Res.* **34**, 100509 (2024).
7. K. H. Bui, T. Yagi, R. Yamamoto, R. Kamiya, T. Ishikawa, Polarity and asymmetry in the arrangement of dynein and related structures in the *Chlamydomonas* axoneme. *J. Cell Biol.* **198**, 913–925 (2012).
8. R. Yamamoto, J. Hwang, T. Ishikawa, T. Kon, W. S. Sale, Composition and function of ciliary inner-dynein-arm subunits studied in *Chlamydomonas reinhardtii*. *Cytoskeleton (Hoboken)* **78**, 77–96 (2021).
9. R. Kamiya, T. Yagi, Functional diversity of axonemal dyneins as assessed by in vitro and in vivo motility assays of *Chlamydomonas* mutants. *Zoolog. Sci.* **31**, 633–644 (2014).
10. L. Newman *et al.*, The impact of primary ciliary dyskinesia on female and male fertility: A narrative review. *Hum. Reprod. Update* **29**, 347–367 (2023).
11. N. Keicho *et al.*, Impact of primary ciliary dyskinesia: Beyond sinobronchial syndrome in Japan. *Respir. Investig.* **62**, 179–186 (2024).
12. K. Takeuchi *et al.*, Practical guide for the diagnosis and management of primary ciliary dyskinesia. *Auris Nasus Larynx* **51**, 553–568 (2024).
13. D. Kobayashi, H. Takeda, Ciliary motility: The components and cytoplasmic preassembly mechanisms of the axonemal dyneins. *Differentiation* **83**, S23–S29 (2012).
14. P. B. Desai, A. B. Dean, D. R. Mitchell, "Cytoplasmic preassembly and trafficking of axonemal dyneins" in *Dyneins: The Biology of Dynein Motors*, (Academic Press, ed. 2nd Edition, 2017), p. 684.
15. D. R. Mitchell, R. Yamamoto, "Chapter 5 - Axonemal dynein preassembly" in *The Chlamydomonas Sourcebook*, S. K. Dutcher, Ed. (Academic Press, ed. 3rd, 2023), pp. 133–155.
16. J. L. Rosenbaum, G. B. Witman, Intraflagellar transport. *Nat. Rev. Mol. Cell Biol.* **3**, 813–825 (2002).
17. N. Klena, G. Pigino, Structural biology of cilia and intraflagellar transport. *Annu. Rev. Cell Dev. Biol* **38**, 103–123 (2022).
18. M. Taschner, E. Lorentzen, The intraflagellar transport machinery. *Cold Spring Harb. Perspect. Biol.* **8**, a028092 (2016).
19. G. R. Mali *et al.*, ZMYND10 functions in a chaperone relay during axonemal dynein assembly. *eLife* **7**, e34389 (2018).
20. H. Fabczak, A. Osinka, Role of the novel Hsp90 co-chaperones in dynein arms' preassembly. *Int. J. Mol. Sci.* **20**, 6174 (2019).
21. B. Braschi *et al.*, Consensus nomenclature for dyneins and associated assembly factors. *J. Cell Biol.* **221**, e202109014 (2022).
22. C. Austin-Tse *et al.*, Zebrafish ciliopathy screen plus human mutational analysis identifies *C21orf59* and *CCDC65* defects as causing primary ciliary dyskinesia. *Am. J. Hum. Genet.* **93**, 672–686 (2013).
23. L. Marie-Hardy, Y. Cantaut-Belarif, R. Pietton, L. Slimani, H. Pascal-Moussellard, The orthopedic characterization of *cfap298*^{tm304} mutants validate zebrafish to faithfully model human AIS. *Sci. Rep.* **11**, 7392 (2021).
24. D. Tang *et al.*, Morpholino-mediated knockdown of ciliary genes in *Euplotes vannus*, a novel marine ciliated model organism. *Front Microbiol.* **11**, 549781 (2020).
25. E. F. Hom *et al.*, A unified taxonomy for ciliary dyneins. *Cytoskeleton (Hoboken)* **68**, 555–565 (2011).
26. S. E. Dougherty, A. O. Maduka, T. Inada, G. M. Silva, Expanding role of ubiquitin in translational control. *Int. J. Mol. Sci.* **21**, 1151 (2020).
27. A. Ciechanover, Intracellular protein degradation: From a vague idea thru the lysosome and the ubiquitin-proteasome system and onto human diseases and drug targeting. *Best Pract. Res. Clin. Haematol.* **30**, 341–355 (2017).
28. Y. T. Kwon, A. Ciechanover, The ubiquitin code in the ubiquitin-proteasome system and autophagy. *Trends Biochem. Sci.* **42**, 873–886 (2017).

29. C. Kennedy, K. McPhie, K. Rittinger, Targeting the ubiquitin system by fragment-based drug discovery. *Front Mol. Biosci.* **9**, 1019636 (2022).
30. X. Sheng, Z. Xia, H. Yang, R. Hu, The ubiquitin codes in cellular stress responses. *Protein Cell* **15**, 157–190 (2024).
31. A. Ciechanover, The unravelling of the ubiquitin system. *Nat. Rev. Mol. Cell Biol.* **16**, 322–324 (2015).
32. X. Li *et al.*, An indexed, mapped mutant library enables reverse genetics studies of biological processes in *Chlamydomonas reinhardtii*. *Plant Cell* **28**, 367–387 (2016).
33. L. Wang, X. Li, G. Liu, J. Pan, FBB18 participates in preassembly of almost all axonemal dyneins independent of R2TP complex. *PLoS Genet.* **18**, e1010374 (2022).
34. I. Minoura, R. Kamiya, Strikingly different propulsive forces generated by different dynein-deficient mutants in viscous media. *Cell Motil Cytoskeleton* **31**, 130–139 (1995).
35. R. Yamamoto, Y. Kitamura, T. Kon, *Chlamydomonas* dynein-preassembly-deficient mutants exhibit characteristic ciliary responses to viscous media. *MicroPubl. Biol.* **2024**, https://doi.org/10.17912/micropub.biology.001149 (2024).
36. R. Kamiya, Analysis of cell vibration for assessing axonemal motility in *Chlamydomonas*. *Methods* **22**, 383–387 (2000).
37. T. Yagi *et al.*, An axonemal dynein particularly important for flagellar movement at high viscosity. Implications from a new *Chlamydomonas* mutant deficient in the dynein heavy chain gene *DHC9*. *J. Biol. Chem.* **280**, 41412–41420 (2005).
38. T. Yagi, R. Kamiya, "9 - Genetic approaches to axonemal dynein function in *Chlamydomonas* and other organisms A2 - King, Stephen M" in *Dyneins* (Academic Press, Boston, 2012), pp. 272–295.
39. S. M. King, T. Yagi, R. Kamiya, "Chapter 4 - Axonemal dyneins: Genetics, structure, and motor activity" in *The Chlamydomonas Sourcebook*, S. K. Dutcher, Ed. (Academic Press, 2023), (ed. 3rd, pp. 79–131).
40. K. M. Jaffe *et al.*, *c21orf59/kurly* controls both cilia motility and polarization. *Cell Rep.* **14**, 1841–1849 (2016).
41. G. M. Penny, S. K. Dutcher, Gene dosage of independent dynein arm motor preassembly factors influences cilia assembly in *Chlamydomonas reinhardtii*. *PLoS Genet.* **20**, e1011038 (2024).
42. R. Kamiya, E. Kurimoto, E. Muto, Two types of *Chlamydomonas* flagellar mutants missing different components of inner-arm dynein. *J. Cell Biol.* **112**, 441–447 (1991).
43. G. Piperno, Z. Ramanis, E. F. Smith, W. S. Sale, Three distinct inner dynein arms in *Chlamydomonas* flagella: Molecular composition and location in the axoneme. *J. Cell Biol.* **110**, 379–389 (1990).
44. Z. L. Payne, G. M. Penny, T. N. Turner, S. K. Dutcher, A gap-free genome assembly of *Chlamydomonas reinhardtii* and detection of translocations induced by CRISPR-mediated mutagenesis. *Plant Commun.* **4**, 100493 (2023).
45. T. Kubo *et al.*, Together, the IFT81 and IFT74 N-termini form the main module for intraflagellar transport of tubulin. *J. Cell Sci.* **129**, 2106–2119 (2016).
46. J. M. Brown, D. A. Cochran, B. Craige, T. Kubo, G. B. Witman, Assembly of IFT trains at the ciliary base depends on IFT74. *Curr. Biol.* **25**, 1583–1593 (2015).
47. X. Zhu, Y. Liang, F. Gao, J. Pan, IFT54 regulates IFT20 stability but is not essential for tubulin transport during ciliogenesis. *Cell Mol. Life Sci.* **74**, 3425–3437 (2017).
48. K. J. Cho *et al.*, ZMYND10 stabilizes intermediate chain proteins in the cytoplasmic pre-assembly of dynein arms. *PLoS Genet.* **14**, e1007316 (2018).
49. R. L. Huizar *et al.*, A liquid-like organelle at the root of motile ciliopathy. *eLife* **7**, e38497 (2018).
50. R. Yamamoto, M. Hirono, R. Kamiya, Discrete PIH proteins function in the cytoplasmic preassembly of different subsets of axonemal dyneins. *J. Cell Biol.* **190**, 65–71 (2010).
51. R. Yamamoto *et al.*, *Chlamydomonas* DYX1C1/PF23 is essential for axonemal assembly and proper morphology of inner dynein arms. *PLoS Genet.* **13**, e1006996 (2017).
52. H. Omran *et al.*, Ktu/PF13 is required for cytoplasmic pre-assembly of axonemal dyneins. *Nature* **456**, 611–616 (2008).
53. H. M. Mitchison *et al.*, Mutations in axonemal dynein assembly factor *DNAAF3* cause primary ciliary dyskinesia. *Nat. Genet.* **44**, 381–389 (2012).
54. R. Yamamoto *et al.*, Mutations in PIH proteins MOT48, TWI1 and PF13 define common and unique steps for preassembly of each, different ciliary dynein. *PLoS Genet.* **16**, e1009126 (2020).
55. B. Huang, G. Piperno, D. J. Luck, Paralyzed flagella mutants of *Chlamydomonas reinhardtii*. Defective for axonemal doublet microtubule arms. *J. Biol. Chem.* **254**, 3091–3099 (1979).
56. H. Sakakibara, D. R. Mitchell, R. Kamiya, A *Chlamydomonas* outer arm dynein mutant missing the α heavy chain. *J. Cell Biol.* **113**, 615–622 (1991).
57. M. Sakato-Antoku, S. M. King, Outer-arm dynein light chain LC1 is required for normal motor assembly kinetics, ciliary stability, and motility. *Mol. Biol. Cell* **34**, ar75 (2023).
58. W. Kabsch, Evaluation of single-crystal X-ray diffraction data from a position-sensitive detector. *J. Appl. Crystallogr.* **21**, 916–924 (1988).
59. W. Kabsch, Automatic processing of rotation diffraction data from crystals of initially unknown symmetry and cell constants. *J. Appl. Crystallogr.* **26**, 795–800 (1993).
60. P. D. Adams *et al.*, PHENIX: A comprehensive Python-based system for macromolecular structure solution. *Acta Crystallogr. D Biol. Crystallogr.* **66**, 213–221 (2010).
61. T. C. Terwilliger *et al.*, Decision-making in structure solution using Bayesian estimates of map quality: The PHENIX AutoSol wizard. *Acta Crystallogr. D Biol. Crystallogr.* **65**, 582–601 (2009).
62. W. Kabsch, C. Sander, Dictionary of protein secondary structure: Pattern recognition of hydrogen-bonded and geometrical features. *Biopolymers* **22**, 2577–2637 (1983).
63. E. Jurrus *et al.*, Improvements to the APBS biomolecular solvation software suite. *Protein Sci.* **27**, 112–128 (2018).
64. D. Eisenberg, E. Schwarz, M. Komaromy, R. Wall, Analysis of membrane and surface protein sequences with the hydrophobic moment plot. *J. Mol. Biol.* **179**, 125–142 (1984).
65. L. Sanchez-Pulido, C. P. Ponting, Extending the horizon of homology detection with coevolution-based structure prediction. *J. Mol. Biol.* **433**, 167106 (2021).
66. S. Vijay-Kumar, C. E. Bugg, W. J. Cook, Structure of ubiquitin refined at 1.8 Å resolution. *J. Mol. Biol.* **194**, 531–544 (1987).
67. L. Cappadocia, C. D. Lima, Ubiquitin-like protein conjugation: Structures, chemistry, and mechanism. *Chem. Rev.* **118**, 889–918 (2018).
68. A. C. O. Vertegaal, Signalling mechanisms and cellular functions of SUMO. *Nat. Rev. Mol. Cell Biol.* **23**, 715–731 (2022).
69. F. Sievers, D. G. Higgins, Clustal omega. *Curr. Protoc Bioinf.* **48**, 1–16 (2014).
70. O. Boix *et al.*, pTINCR microprotein promotes epithelial differentiation and suppresses tumor growth through CDC42 SUMOylation and activation. *Nat. Commun.* **13**, 6840 (2022).
71. J. Jumper *et al.*, Highly accurate protein structure prediction with AlphaFold. *Nature* **596**, 583–589 (2021).
72. M. Sakato-Antoku, S. M. King, Developmental changes in ciliary composition during gametogenesis in *Chlamydomonas*. *Mol. Biol. Cell* **33**, br10 (2022).
73. S. D. Gallaher, S. T. Fitz-Gibbon, A. G. Glaesener, M. Pellegrini, S. S. Merchant, *Chlamydomonas* genome resource for laboratory strains reveals a mosaic of sequence variation, identifies true strain histories, and enables strain-specific studies. *Plant Cell* **27**, 2335–2352 (2015).
74. R. J. Craig *et al.*, The *Chlamydomonas* genome project, version 6: Reference assemblies for mating type plus and minus strains reveal extensive structural mutation in the laboratory. *Plant Cell* **35**, 644–672 (2022).
75. E. H. Harris, *The Chlamydomonas Sourcebook: A Comprehensive Guide to Biology and Laboratory Use* (Academic Press, San Diego, 1989), p. 780.